Journal of Archaeological Science 37 (2010) 3000–3009

Contents lists available at ScienceDirect

Journal of Archaeological Science

journal homepage: http://www.elsevier.com/locate/jas

Iron Age hydraulic plaster from Tell es-Safi/Gath, Israel

Lior Regev [a], Alexander Zukerman [b], Louise Hitchcock [c], Aren M. Maeir [d], Steve Weiner [a], Elisabetta Boaretto [d,e,*]

[a] Department of Structural Biology and the Kimmel Center for Archaeological Science, Weizmann Institute of Science, Rehovot 76100, Israel
[b] W.F. Albright Institute of Archaeological Research, P.O. Box 19096, 91190 Jerusalem, Israel
[c] Centre for Classics and Archaeology, University of Melbourne, Parkville, 3010 Victoria, Australia
[d] Department of Land of Israel Studies and Archaeology, Bar-Ilan University, Ramat-Gan 52900, Israel
[e] Radiocarbon and Cosmogenic Isotopes Laboratory, Kimmel Center for Archaeological Science, Weizmann Institute of Science, 76100 Rehovot, Israel

ARTICLE INFO

Article history:
Received 21 December 2009
Received in revised form
9 June 2010
Accepted 23 June 2010

Keywords:
Hydraulic plaster
Israel
Philistia
Iron Age
Tell es-Safi/Gath
Aegean

ABSTRACT

Hydraulic plasters or mortars prior to the Roman period are rare. Here, we report the identification and characterization of 3000 year old (Iron Age) hydraulic plaster surfaces from the site of Tell es-Safi/Gath. This site, located in central Israel, was occupied almost continuously from prehistoric through modern times, and is identified as the Canaanite and Philistine city of Gath. A survey using an on-site Fourier transform infrared spectrometer (FTIR) identified the presence of amorphous silicates, in addition to calcite, in each of two superimposed plaster layers. This suite of minerals is characteristic of hydraulic plaster. An in-depth characterization of the plasters using FTIR, acid dissolution, X-ray fluorescence (XRF), X-ray powder diffractometry (pXRD), heating experiments and scanning electron microscopy (SEM) coupled with energy dispersive spectroscopy (SEM–EDS), shows that special silicate-containing minerals were brought from some distance to the site in order to produce these plaster surfaces. We therefore conclude that the plasters were deliberately produced, and were not the result of a fortuitous addition of local silicate minerals. A layer of around 150 μm thick enriched in carbonate hydroxylapatite was found in both plaster surfaces, and the same mineral was identified by infrared spectrometry in the surrounding sediments. This suggests that organic materials were used on these surfaces. These surfaces are among the oldest hydraulic plasters known.

1. Introduction

Lime plaster was developed at least 15,000 years ago during the Natufian period and was extensively used during the Neolithic in the Near East (Gourdin and Kingery, 1975; Kingery et al., 1988; Wright, 2000, 2005; Valla et al., 2007). Since its invention, the basic preparation methods remained unchanged. Calcite, usually in the form of limestone, is heated to around 800 °C. This causes the release of carbon dioxide in a process known as 'calcination', and the production of calcium oxide (CaO, 'quicklime'). The quicklime is not stable and readily hydrates to form calcium hydroxide ($Ca(OH)_2$, slaked lime or portlandite). The latter absorbs carbon dioxide from the atmosphere and calcite is reformed. During the drying process, the plaster hardens.

A second type of plaster, which can harden under water, is called 'hydraulic plaster'. Hydraulic plaster is obtained when slaked lime is mixed with highly disordered silicate minerals. The Romans used volcanic ash from the area of Pozzuoli (ancient Puteoli) in the Bay of Naples, and hence this class of additives is known as 'pozzolanic additives' (Borrelli, 1999). This plaster was first documented in Classical-period Greece (5th to 4th centuries BCE), and was widely used by the Romans, from the 2nd century BCE onwards, and in post-Roman periods (Ward-Perkins, 1981, 97–120). Its ability to set under water enabled the building of harbors and bridges. A description of hydraulic plaster preparation using pozzolanic additives was written by Vitruvius (De Architectura 2.6), some 2000 years ago.

The origin and early development of hydraulic plaster technology is obscure. One reason is the manner in which these materials are described and analyzed. Several studies report pre-Roman "hydraulic" plasters, but these identifications are problematic, particularly since most of them lack a proper description and analysis of physicochemical properties of these materials, and others refer to materials different from true hydraulic plaster. One

* Corresponding author. Radiocarbon and Cosmogenic Isotopes Laboratory, Kimmel Center for Archaeological Science, Weizmann Institute of Science, 76100 Rehovot, Israel. Tel.: +972 8 934 3213; fax: +972 8 934 6062.
E-mail address: elisabetta.boaretto@weizmann.ac.il (E. Boaretto).

0305-4403/$ – see front matter © 2010 Elsevier Ltd. All rights reserved.
doi:10.1016/j.jas.2010.06.023

such case is the so-called 'white ware' vessels from Tell Ramad (Syria) from 5900 BCE (Gourdin and Kingery, 1975). No supporting evidence for a pozzolanic reaction was provided (Kingery et al., 1988). An even older plaster sculpture from the Pre-Pottery Neolithic Jericho (ca. 7000–6000 BCE) was described as having a 'limy clay' binder (Kingery et al., 1988). A plastered floor from Kommos, Crete, dated to the Middle Minoan III period (17th century BCE), was analysed and described as 'cement with a very high hydraulicity' (Dandrau and Dubernet, 2006). However, the authors suggest that the builders used marl (limestone with 35–65% clay) as their calcite source mainly because of its natural abundance locally and not specifically because of its physicochemical properties. The excavators at Phaistos applied the terms "calcestruzzo" or "astráki" to a type of cement described as "slightly hydraulic" and composed of stones, clay, lime, crushed potsherds, and sometimes whole pots (Fiandra, 1961–1962: 123, 125–126; Levi, 1964: 3–4). It was used to create a platform covering the remains of the "First Palace" prior to the construction of the "Second Palace" in Middle Minoan III/Late Minoan IA (ca. 1700 BCE; see Shaw, 1971: 222–223 with references; Walberg, 2001: 13). Chiotis et al. (2001) analyzed Mycenaean mortars and waterproofing plasters on the Greek mainland. The samples included plasters from cisterns of the citadel at Mycenae and at the Argive Heraion, and the floor of the courtyard in the palace of Tiryns. The plasters consist of an undercoat made of one or two successive layers, covered by a thin superficial lining, either homogeneous or stratified, composed of two layers. A siliceous lining was found in all three samples, together with some calcite, gypsum and clay minerals. The undercoats from Tiryns and Heraion are composed of lime with fragments and powdered terracotta, which can function as a pozzolanic material. This study indicates that hydraulic plaster was used during the time period of the Aegean civilization, providing chronological continuity in the Minoan and Mycenaean periods in the Aegean. The Mycenaean adaptation of Minoan building technologies has been thoroughly studied (for example, Wright, 1978), and it is highly likely that plaster technology was transmitted elsewhere. Furlan and Bissegger (1975) described lime mortars containing crushed ceramics from the 10th century BCE from Jerusalem. Some samples of wall plaster from the Iron Age II Tall Jawa contained silicate inclusions, but their composition or source were not fully determined (Hancock, 2003: 459–460).

The rarity of reports on pre-Roman hydraulic plasters can be due to the possibility that this plaster type was not widely used, or because they were not properly identified, or both. Hydraulic plaster cannot be identified only by visual inspection. A laboratory analysis is required.

We present here the identification and detailed analysis of two superimposed hydraulic plaster surfaces from Tell es-Safi/Gath. Tell es-Safi/Gath is a 50 ha mound in central Israel (Fig. 1), identified as the Canaanite and Philistine city of Gath (Maeir, 2008). The site has been excavated regularly since 1996 by the Tell es-Safi/Gath Archaeological Project of the Institute of Archaeology, Bar-Ilan University, directed by A.M. Maeir. The site was settled almost continuously from the Chalcolithic period till modern times, with several occupation peaks, one of which is during the Iron Age (12th to 8th centuries BCE). Several Iron Age strata were uncovered, representing most of the developmental stages of the Philistine material culture.

2. Materials and methods

2.1. Archaeological context and description

Two plaster surfaces with a combined thickness of about 20 cm, were found in Area A, in square 223/80C (Fig. 2a). The surfaces were

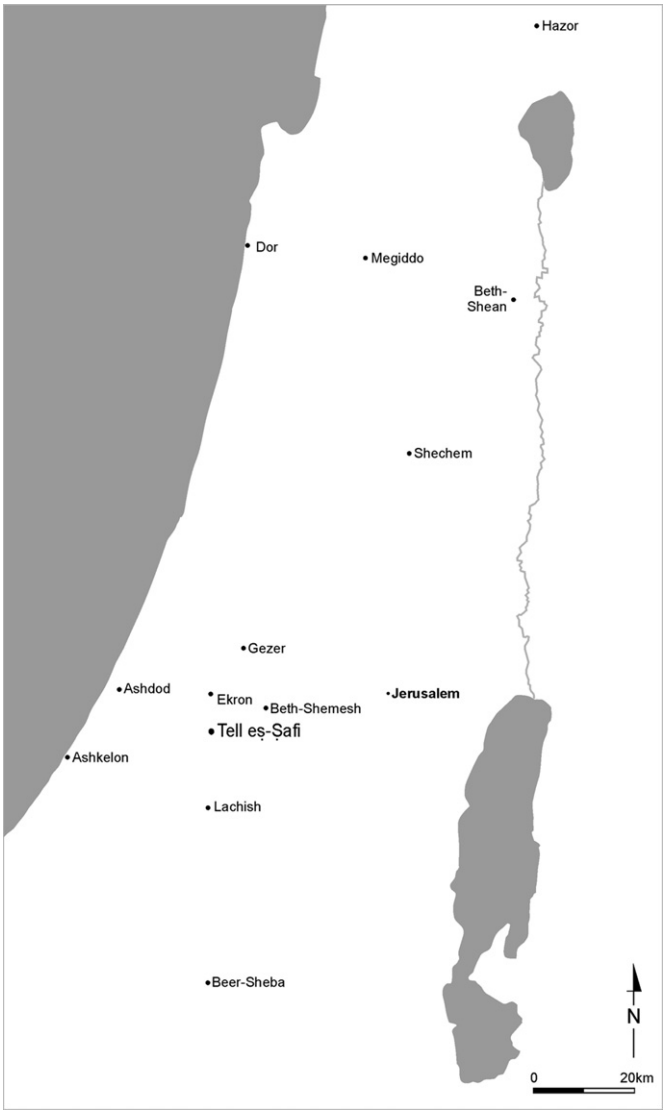

Fig. 1. Map of Israel with location of Tell es-Safi/Gath and major Iron Age sites.

located in the north-western corner of the square, without any clear structural relations to adjacent features (Fig. 2b). Although all the edges of the surfaces are eroded or cut, and their original extent is unknown, the top of both surfaces were smooth and flat; an effect that might be achieved by means of a stone float (Shaw, 1971, 210, Fig. 238, 214). The measurements of the irregularly shaped preserved patch are ca. 120 × 75 cm. The series of preparation layers below the lower surface (L122036) indicates that more care and attention was paid to the construction of the lower surface than the upper surface. The base of the lower surface is composed of two layers of cobbles. The uppermost one (L122039), consists of approximately one hundred cobbles each measuring 6–10 cm, and the lower one was left in situ and was partially exposed. This was overlaid by a 5 cm thick layer of dark brown heavy clay (L122038), that was not exposed to elevated temperatures based on its infrared spectrum (Berna et al., 2007). An additional preparation layer, around 5 cm thick, was laid down on the clay layer (L122036, 2nd layer). This layer has a similar composition to the overlying plaster surfaces. However, in contrast to the surfaces, this layer is fragile and contains a very large amount of water-worn mollusk shell fragments (under 1 cm in size, averaging 7 mm). In addition, several hard usually black colored porous pieces, around 5 cm in

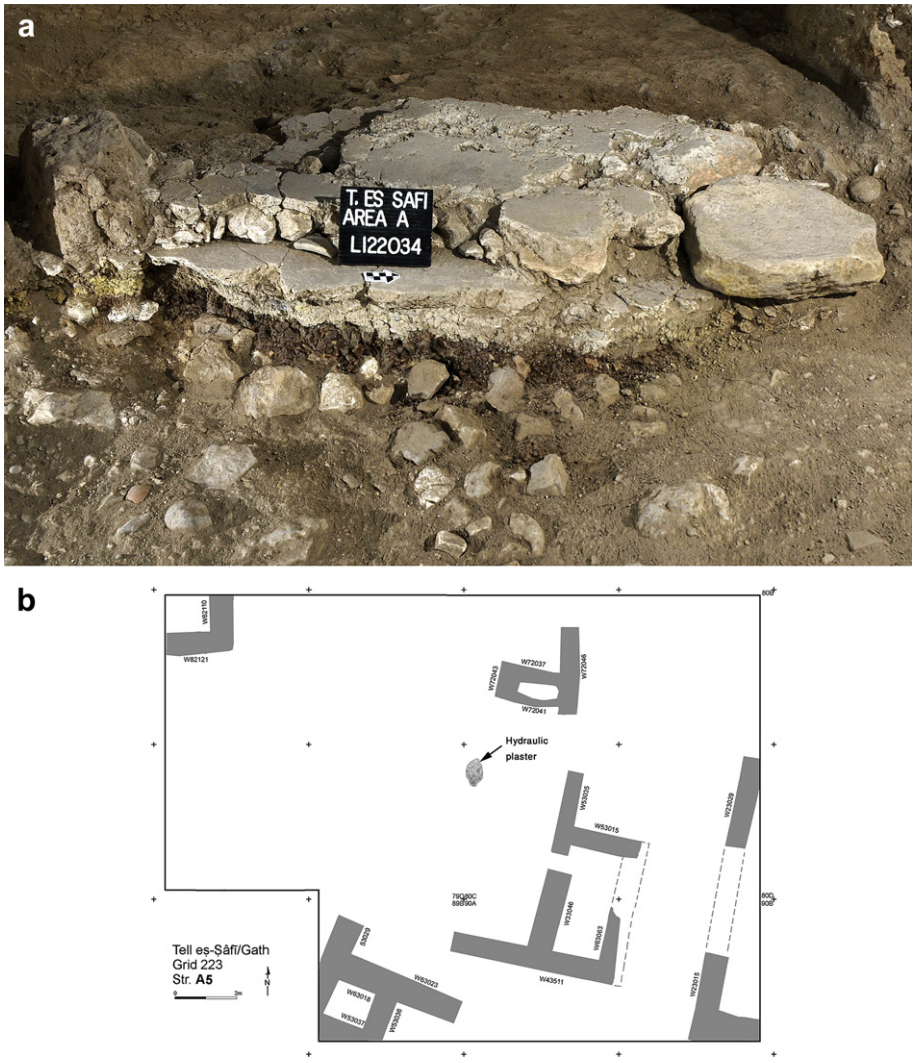

Fig. 2. Tell es-Safi/Gath – (a) photograph of the plaster surfaces from excavation square 223/80c, looking west. Locus 122034 refers to the upper surface. The brick-like feature on the left is artificial and was left as a sample for micromorphology. Scale is 5 cm. The picture was taken by Richard Wiskin. (b) A schematic plan of the central part of Area A, local Stratum A5 (by J. Rosenberg and A. Zukerman).

size, were present. The southern part of this layer has a yellow color (left end in Fig. 2a). The lower plaster surface (L122036, 1st layer) is about 3 cm thick, and is dense and hard with a flat upper interface. The western end of this surface (far end in Fig. 2a) slopes or laps slightly upward. This may indicate the former existence of a wall, or could result from the placement of a temporary wooden slat used as a guide to indicate where the process of plastering should end (Shaw, 2006: 207). When the upper plaster surface (L122034) was constructed, the lower surface was covered by a thin layer of brown, powdery soil (not heated, based on infrared spectroscopy), followed by a layer of cobbles, 5–10 cm thick and containing some flat pottery sherds. Some larger flat stones were also incorporated, with the largest one (B1220209, visible on the rightmost side at Fig. 2), measuring 32 × 23 cm. Our analysis showed that it had traces of attached plaster. The upper surface (L122034) is as dense, hard and flat as the lower surface. All of the layers slope slightly downward from the south-west to the north-east.

All plaster samples and some of the surrounding sediments, including samples from sediments up to 8 cm above the upper surface, contained carbonate hydroxylapatite peaks in their infrared spectra. The source of the phosphate is most likely from decayed organic material overlying the plaster surfaces. No *in situ* finds were associated with these surfaces, besides an accumulation of extensively burned and calcined bones of a caprid (carpal, first phalanx, and unfused shaft) and a cow (proximal ulna), found on both the upper surface and the lower surface in an area where the upper surface was missing.

The plaster surfaces pre-date the 9th century BCE (late Iron Age IIA) Stratum A3, as its walls and floors are well above the plaster and related elements. Because of the limited horizontal extent of the exposure, the pre-Stratum A3 remains in this part of Area A cannot yet be physically linked to contemporary remains uncovered elsewhere, and the area-wide stratigraphic sequence is yet to be established. Within the local stratigraphic sequence for this part of the area, the plaster belongs to Stratum A5. However, based on ceramic evidence from this stratum, as well as from similar assemblages retrieved from other parts of the excavation area, the plaster surfaces date to the late Iron Age I, that is, to the late 11th to early 10th century BCE (for detailed discussions see Maeir et al., 2008; Zukerman and Maeir, in press).

2.2. Fourier transform infrared spectrometry (FTIR)

A few milligrams of sample were homogenized and powdered in an agate mortar and pestle. About 0.3 mg were left in the mortar and mixed with about 40 mg of KBr and pressed into a 7 mm pellet using

a hand press (Qwik Handi-Press, Spectra-Tech Industries Corporation). Infrared spectra were obtained at 4 cm^{-1} resolution for 32 scans. FTIR analyses on-site were made using a Nicolet IR100 (Thermo), or in the laboratory using a Nicolet 380 (Thermo). The ν_2/ν_4 ratios for the calcite samples were determined following the method of Chu et al. (2008), paying careful attention to the width at half height of the ν_3 peak.

2.3. Plaster embedding for FTIR analysis

A piece of plaster (roughly 5 × 5 cm) was embedded in 1 l of 4:1 polyester to acetone mix with 15 ml of hardener, and left to cure for about two weeks. After full hardening, the block was cut using a rock saw to 70 × 50 × 30 mm, leaving the surface of the plaster intact. The slice was attached to a 76 × 50 mm microscope slide using Crystalbond 509-3 (Ted Pella, INC.), and sawed to a 1 mm thick slice using a PetroThin – Thin Sectioning System (Buehler). The slice was detached from the glass slide by heating and remains of the Crystalbond were cleaned using an ultrasonic cleaner (Branson, 1510) in acetone. Features for sampling were extracted using a hand held grinding tool (Wolf). The powder was analyzed by FTIR as described above.

2.4. Acid dissolution

Three crushed plaster samples of 3.6–3.7 g each were treated for 2 days with an excess of one of the following concentrated acids: hydrochloric acid (32%), phosphoric acid (85%) and acetic acid (99%). The samples were then washed and dried.

2.5. X-ray powder diffractometry (XRD)

About 0.5 g of plaster were lightly crushed and macroscopic aggregates were removed. Analysis was carried out using a Rigaku Ultima III instrument, with Cu-Kα radiation. Powdered samples were measured in the range of two-theta (8–60 degrees), at a rate of 0.5 degree per min, and a sampling interval of 0.05.

2.6. Heating plaster

2–4 g of crushed chalk and plaster samples and 1 g from the acetic acid insoluble fraction were heated to different temperatures (500 °C, 700 °C, 900 °C or 1100 °C) in an oven for 4 h, left to cool overnight and analyzed by FTIR spectrometry the next day.

2.7. Scanning electron microscopy–energy dispersive spectroscopy (SEM–EDS)

Samples were cut using a diamond-coated saw (PetroThin, Buehler), after mounting in Epoxy resin. They were then ground, polished and carbon coated. Grinding was done first with a Diamond grinding disk (Ultra-Prep 45 μm from Buehler) followed by a series of SiC papers (P1000, P1200, P2400, P4000). Polishing was done with diamond solutions of 3 μm (DiaPro Dac from Struers) and 1 μm (DiaPro NapB from Struers). Each grinding and polishing step lasted for several minutes. Analyses of the microstructure, mineralogy and chemical composition of the samples were carried out using a LEO 55VP SEM equipped with an Oxford INCA Energy Dispersive Spectrometer (EDS). EDS analyses were carried out at 15 kV and at a working distance of 8 mm. Counting time was 100 s. Images were obtained using a back-scattered electron detector. Measurements were made using stored virtual standard data, after calibration with a titanium standard, and normalization of the collected elemental concentrations to 100%.

2.8. X-ray fluorescence (XRF)

Quantitative bulk chemical analyses were performed by energy dispersive X-ray fluorescence (ED-XRF), using a Spectro-XEPOS bench top instrument, with a Palladium (Pd) anode, equipped with a series of secondary targets. Samples of approximately 3 g each were homogenized by mortar and pestle and measured as powders in air environment. Accuracy is estimated to be better than 10% for most elements present at concentrations above 5%. Elements lighter than aluminium cannot be measured.

3. Results

3.1. FTIR spectrometry of the plaster binder

The plaster surfaces have a significantly different infrared spectrum from common lime plaster (Fig. 3a). Calcite is the main component of lime plasters (absorption peaks at 1450, 874 and 712 cm^{-1}), but is only a minor component of these plasters. The major component of the binder of these plasters has a broad strong absorption peak between 1040 cm^{-1} and 1060 cm^{-1} and a minor peak at 464 cm^{-1} (Fig. 3d–f). The latter is characteristic of silicate minerals. Pozzolana, an aluminosilicate rich volcanic ash used to produce Roman hydraulic plaster, has a broad IR absorption peak at 1036 cm^{-1} (Fig. 3b). In fact the spectra from the Iron Age plaster layers are similar, but not identical to the infrared spectrum of Roman hydraulic plaster (Fig. 3c). We regard the similarity in infrared spectra between Roman hydraulic plaster and the plasters from Tel es Safi as one of the major reasons why the Iron Age plasters can be defined as hydraulic plasters. An interesting feature of the spectra of these plasters is the presence of a weak broad peak around 800 cm^{-1}, suggesting that the material may include a highly disordered silicate. An identical peak is present in amorphous silica (Fig. 3g), as opposed to quartz which has a characteristic doublet (779 cm^{-1} and 797 cm^{-1}) at this location. The major absorption peak of opal is however around 1100 cm^{-1}. The presence of small peaks at 605 cm^{-1} and 565 cm^{-1} indicates the presence of carbonate hydroxylapatite (Fig. 3e and f).

The ratio of the 875 cm^{-1} and 712 cm^{-1} peaks of calcite (ν_2/ν_4 ratio) is a reflection of the extent of disorder in the calcite crystal lattice (Gueta et al., 2007; Chu et al., 2008). The ν_2/ν_4 ratios of these plasters are 6.8 for the upper surface and 7.8 for the lower one. These are extremely high values, and are similar to the values of newly formed lime plaster. The calcite component of these plasters is therefore highly disordered and this is consistent with the plaster having been prepared from calcium oxide produced by burning limestone. The presence of a disordered silicate phase, as well as disordered calcite, demonstrates that these surfaces are composed of hydraulic plaster. The following is a more detailed characterization of these hydraulic plasters.

3.2. Acid dissolution

Treatment of a sample of hydraulic plaster with 5 N HCl resulted in a weight loss of about 40%. This implies that the calcite and the carbonate hydroxylapatite together comprise less than 40% of the sample. An infrared spectrum of the insoluble residue shows that the main peak shifted from 1060 cm^{-1} to 1082 cm^{-1}. This phase therefore also changed as a result of exposure to acid. Twenty-five grams of the plaster were treated with 5 N HCl and the volume of CO_2 gas was collected and measured. Assuming all this gas was derived from calcite, this implies that about 20% by weight of the plaster is calcite. As some of the gas was derived from carbonate hydroxylapatite, the calcite content must be even lower. We therefore conclude that the major component of this plaster is the

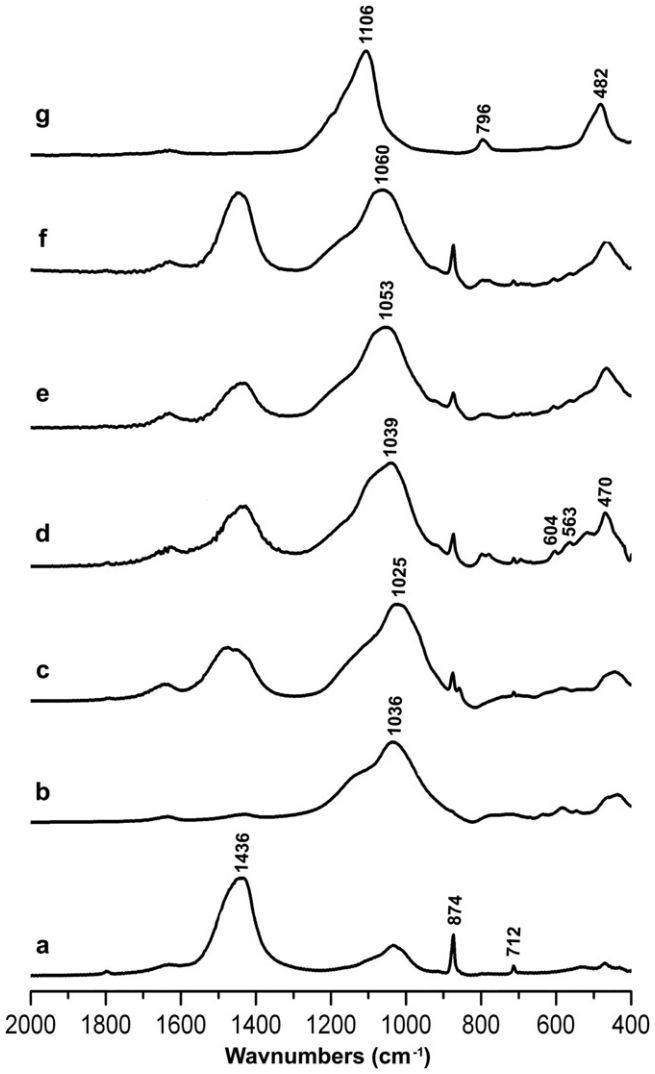

Fig. 3. FTIR analyses of the upper and lower plaster surfaces, and standards for comparison. (a) A typical spectrum of a lime plaster. (b) Spectrum of pozzolana (Bacoli, Pozzuoli, courtesy of P. Tiano). (c) Pozzolanic Roman hydraulic plaster (Augustus Bridge 27BC, courtesy of P. Tiano). (d) Upper interface of the lower plaster surface. (e) Bulk of the lower plaster surface. (f) Bulk of the upper plaster surface. (g) Spectrum of opal (Thousand Oaks, California).

silicate phase which in part is soluble in acid, and calcite is a minor component.

We also treated the hydraulic plaster with phosphoric and acetic acids and analysed the residues using infrared spectroscopy. The phosphoric acid residue had the same spectrum as the HCl treated sample, but the acetic acid residue still contained a major peak at the same location as the untreated sample. Acetic acid therefore does not alter the silicate phase.

3.3. X-ray fluorescence

The major elemental compositions of the different layers are shown in Table 1.

The XRF results confirm that silicates are the major component in the plaster surfaces, while calcium is the minor component. Both surfaces have essentially the same bulk composition. Their Si/Al ratios are around 8.6, whereas the Si/Al ratio of the underlying clay-rich layer at the base is 3.2. This implies that the silicates in the plasters are not derived directly from this clay, and most likely not from other added clay components.

Table 1
Compositional analyses of the various surface layers. The 'yellow layer' refers to a yellow patch at the level of the lower surface, shelly layer, and can be seen in Fig. 1. The 'Black porous' refers to hard pieces, about 5 cm in size, that were found at the same level.

Description	Sample number	Al_2O_3 [%]	SiO_2 [%]	P_2O_5 [%]	K_2O [%]	CaO [%]	Fe_2O_3 [%]
Upper surface	TS9120	6.61	57.45	2.94	2.79	27.03	3.17
Lower surface, upper layer	TS9131-1st	6.08	51.85	3.10	2.84	32.90	3.23
Lower surface, shelly layer	TS9131-2nd	8.82	57.50	3.84	3.27	22.55	4.02
Yellow layer	TS9138	9.90	70.63	4.72	3.48	7.02	4.24
Black porous a	TS9142a	7.52	62.68	3.70	4.81	17.38	3.92
Black porous b	TS9142b	6.81	62.26	2.78	4.48	20.01	3.66
Brown layer	TS9136	18.51	58.96	0.25	2.08	11.73	8.46

3.4. Powder X-ray diffraction

We analyzed the diffraction patterns of the untreated plaster binder and the acetic acid treated binder. The acetic acid removes calcite and possibly other acid soluble phases, but does not affect the major silicate phase based on the infrared spectrum. Six crystalline minerals were identified in the hydraulic plaster binder: calcite, quartz, chlorapatite and/or carbonate hydroxylapatite, analcime, diopside and cristobalite (Fig. 4). Calcite, quartz and carbonate hydroxylapatite were also identified using infrared spectroscopy (Fig. 3 and Table 2). Note that an amorphous mineral phase is not readily detected using X-ray diffraction except for a broad rise in the baseline.

3.5. Heating of the plaster samples

In order to better characterize the amorphous/disordered silicate phase(s), we heated the sample to various temperatures and analysed the products using FTIR (Fig. 5). The reason is that the

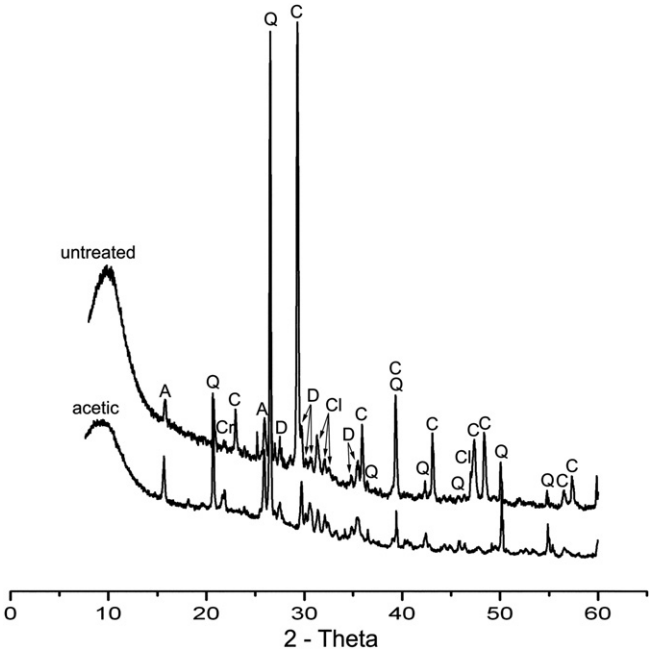

Fig. 4. Powder X-ray diffraction pattern of the untreated and acetic acid treated insoluble fine-grained plaster fractions. (C) calcite $CaCO_3$, (Q) quartz SiO_2, (A) analcime $NaAlSi_2O_6 \cdot H_2O$, (Cr) cristobalite SiO_2, (D) diopside $CaMgSi_2O_6$, (Cl) chlorapatite $Ca_5(PO_4)_3Cl$.

Table 2
Identification of the major mineral components shown in Fig. 6 using infrared spectroscopy.

Feature	Symbol (Fig. 6)	FTIR results
Binder – bulk	N	Pyrogenic calcite, the disordered silicate phase and some quartz.
Binder – surface	H	Pyrogenic calcite and the disordered silicate phase.
Binder – white component	B	Disordered silicate phase with quartz and pyrogenic calcite.
Clays/crushed ceramics	A, J, L	Burnt clay/crushed ceramic, including some calcite and quartz.
Dark colored aggregates	C, D	Geogenic (C) and pyrogenic (D) calcite.
Light colored aggregates	E, G, K, O	Geogenic (E,K) and pyrogenic (G) calcite; quartz (O).
Shell	M	Aragonite
Porous green areas	F, I	Mainly a silicate phase with little calcite and phosphate.

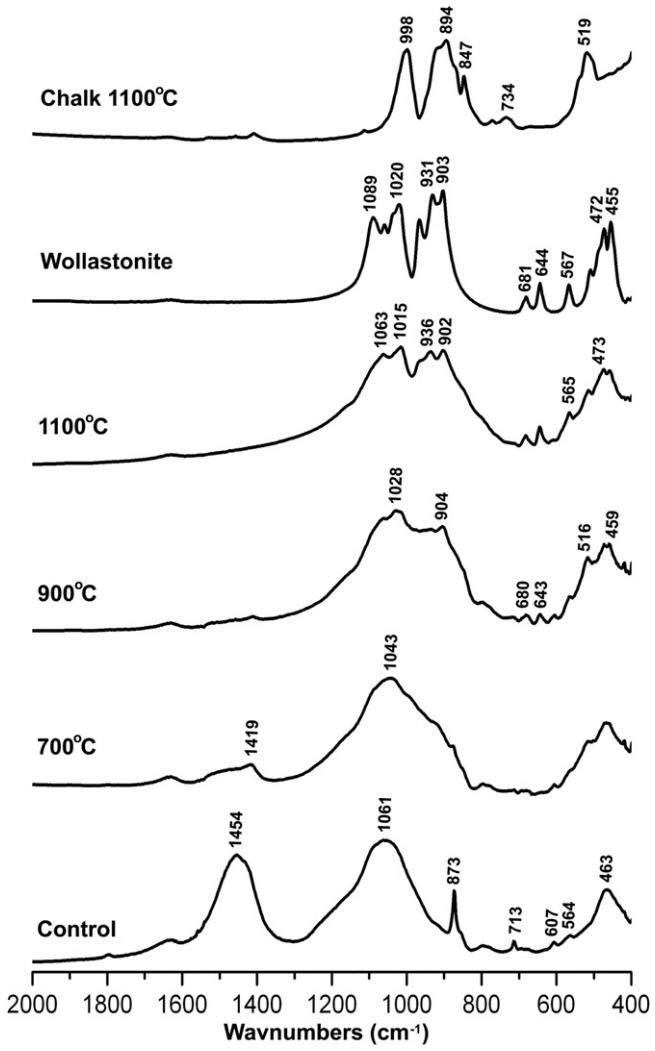

Fig. 5. FTIR spectra of the heated hydraulic plaster samples and the unheated control. The plaster was crushed and heated to the above temperatures for 4 h. FTIR analysis was conducted the following day. The uppermost spectrum is of the local chalk heated to 1100 °C. A spectrum of a wollastonite standard is also shown.

heated sample may crystallize and the crystalline product is more easily identified. This then provides compositional information on the disordered phases. The spectra obtained after heating to 700 °C show the expected breakdown of calcite, which begins around 700 °C, and the appearance of a sharp peak of $Ca(OH)_2$ at 3643 cm^{-1} (not shown here), a shift of the main silicate peak from 1060 cm^{-1} to 1047 cm^{-1} and the appearance of peaks at 517 cm^{-1} and 461 cm^{-1}. The characteristic doublet of the quartz mineral at 797 cm^{-1} and 779 cm^{-1} is not well separated; evidence of a relatively disordered state. The spectra obtained after heating to 900 °C and 1100 °C show the lack of the $Ca(OH)_2$ peak and the presence of a calcium silicate phase. A comparison of the 1100 °C spectrum to a standard spectrum of crystalline wollastonite ($CaSiO_3$) supports the formation at 900 °C and 1100 °C of a disordered wollastonite phase.

One method of inadvertently obtaining a natural hydraulic plaster is to heat calcitic rocks, which have a major clay component, to above 1000 °C. When the local chalk rock was heated to 1100 °C, a spectrum quite different from that of the hydraulic plaster was obtained (Fig. 5). This spectrum includes two major peaks at 894 cm^{-1} and 998 cm^{-1}, as well as minor peaks at 1409 cm^{-1} and 3641 cm^{-1}, typical of calcination of calcite (both appear also in the sample heated to 700 cm^{-1}). Therefore, the silicate source material for the hydraulic plaster could not be the local chalk alone.

3.6. FTIR analysis of binder and aggregates

In order to analyze the aggregates and the binder separately, we embedded a sample of the hydraulic plaster in polyester, and produced a 1 mm thick slice by sawing with a water-cooled saw (Fig. 6). Various distinct features were extracted mechanically (labeled A–N in Fig. 6) and the mineral components were analyzed using FTIR spectrometry. The results are listed in Table 2. The differentiation of pyrogenic and geogenic calcites is based on the ν_2/ν_4 ratio as defined in Chu et al. (2008).

The three binder samples are composed of the disordered silicate phase, pyrogenic calcite and some quartz. Aggregate components (A, J, L in Fig. 6) are either composed of burned clay or crushed ceramics fragments. It is difficult to distinguish between these two options by FTIR alone. A petrographic microscope analysis of a thin section from the same area as the sample shown in Fig. 6, revealed that the quartz particles in feature A all have a similar size, which is typical of a deliberately produced ceramic material (Karkanas Panagiotis, personal communication). Furthermore, it seems that the ceramic fragments were added after the calcination process, since their infrared spectra do not show the characteristic in changes in the structure of clay heated to at least 800 °C (Berna et al., 2007); the temperature required for

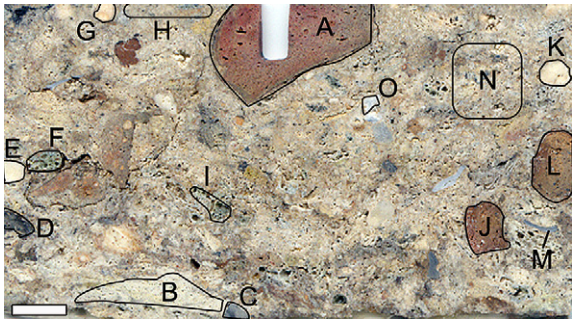

Fig. 6. Photograph of the surface of a plaster sample. The surface of the sample is at the top. The areas analyzed by infrared spectroscopy are outlined and labeled with letters. Scale is 0.5 cm.

calcination. Geogenic calcite aggregates may also have been added after the calcination step, as is common in the production of lime plasters. It is, however, possible that these are limestone fragments of the original rock that were not fully calcined. As quartz is not abundant in the vicinity of the site, the presence of quartz grains in the hydraulic plaster suggests that they were deliberately added from another source. One possible local source was found to have quartz grains of a different size range.

Shells in archaeological sites are commonly composed of aragonite. Since aragonite and calcite have the same chemical composition of $CaCO_3$, and since calcite is more stable than aragonite, aragonitic shells can serve as preservation indicators (Karkanas et al., 2002). Furthermore, aragonite shells transform to calcite when heated to 400 °C (Boynton, 1980), so the presence of an aragonitic shell in the plaster shows that the shells were added after the heating process. The porous green areas are morphologically similar to the black porous pieces analyzed by XRF (Table 1). A dark grey porous piece from the plaster (not in the above section) was analyzed using infrared spectroscopy and powder X-ray diffraction. In both analyses, spectra similar to the acetic acid treated sample (Fig. 4) were obtained. The spectra contained cristobalite and a small amount of calcite.

3.7. SEM–EDS imaging of fine-grained aggregates and the binder

Imaging the plaster using a SEM equipped with a back-scattered electron (BSE) detector and an EDS detector enabled us to analyze aggregates smaller than 1 mm, as well as the binder itself (Fig. 7). Fig. 7a is a BSE image of the polished surface of the hydraulic plaster. Using the EDS device we color-coded the three most abundant elements to produce (Fig. 7b): silicon (Si) in red, calcium (Ca) in green, and aluminum (Al) in blue. Calcium is present only in the fine binder, whereas silicon is present in the binder and in the aggregates. Aggregates that contain only silicon (dark red) are assumed to be composed of quartz ('Q' in Fig. 7b), and those that contain both silicon and aluminum (pinkish color due to red and blue mix) are assumed to be composed of clay ('Cy' in Fig. 7b). The irregular phase around cavities is composed mainly of silicon, with smaller amounts of aluminum. The three highly contrasting fragments (white in the BSE image) are composed mainly of Ti–Fe, Cr–Fe–Al and Si–Zr from left to right respectively. Note that in elemental composition analyses of fairly large areas (not a specific location or feature), the calcium to silicon proportions were around 1:1. This is consistent with finding that upon heating, the binder phase transformed into disordered wollastonite, which also has Ca:Si proportions of 1:1 (Fig. 5).

In order to better characterize the binder phase, we examined the sample at higher magnifications (Fig. 7c and d). In Fig. 7c numerous calcitic particles, ca. 5 μm in size, were detected. However, in other areas such particles were not common. The binder is composed of three phases (Fig. 7d): a Ca-rich phase (green arrows), a Si-rich phase (red arrows), and a phase which has Ca:Si in proportions of 0.5–2 (yellow arrows). We noted in this and other images, that the third phase is sometimes located between the other two phases, raising the possibility that this phase is the product of a reaction between the silicon-rich and calcium-rich phases. Representative elemental analyses of the third phase calcium silicates are shown in Table 3. Compounds 1–7 are roughly 1 micron in size and have irregular shapes. Compounds 8–11 were identified in the acetic acid insoluble fraction. No compounds with calcium to silicon ratio between 0.5 and 2 were identified in the phosphoric acid insoluble fraction.

3.8. The formation of carbonate hydroxylapatite in the plaster surface

Infrared analysis identified carbonate hydroxylapatite in the plaster surface (Fig. 3). Carbonate hydroxylapatite was also identified in the acetic acid insoluble fraction by infrared spectroscopy and by SEM–EDS, and was present in the fine-grained fraction

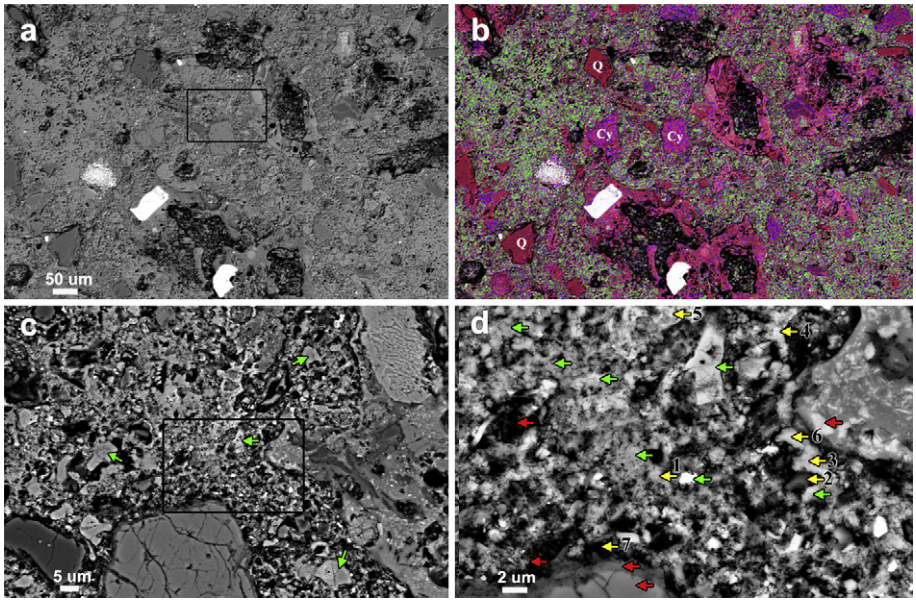

Fig. 7. Representative SEM–EDS analysis of the fine aggregates and the binder. (a) SEM image using a BSE detector of a representative field of the plaster binder. The rectangle marks the magnified area shown in panel c. (b) Same image, analyzed using an EDS device and color coded as follows: calcium (green), silicon (red) and aluminum (blue). The combination of silicon and aluminum produces a pink color. "Q" marks representative silicon only particles, assumed to be quartz. "Cy" marks representative high silicon and aluminum particles, assumed to be clay. (c) Magnification of the area marked by a rectangle in a. Several 5–10 μm calcite particles are marked with green arrows. The rectangle marks the area magnified in panel d. (d) High magnification image of the fine binder phase. Green arrows represent measurements with stoichiometric Ca:Si ratios over 4, yellow arrows represent ratios between 0.5 and 2 and red arrows mark measurements with Ca:Si ratios below 0.2. Elemental analyses of the areas designated by the yellow arrows are shown in Table 3.

Table 3
Elemental analyses of the hydraulic phase. The values represent atomic percentages. Numbers 1–7 relate to the measurements marked by yellow arrows in Fig. 7d. Numbers 8–11 were identified in the acetic acid insoluble fraction.

	Si	Ca	Al	Mg	P	K	Fe	Ca/Si	Ca/Al
1	9.0	18.1	0.5	0.8	0.4	0.3	0.2	2.0	40.1
2	8.7	15.8	1.0	1.8	0.3	0.5	0.3	1.8	16.2
3	10.6	17.3	1.0	1.2	0.7	1.1	0.6	1.6	17.0
4	12.7	14.9	1.5	3.4	0	0.5	0.8	1.2	9.8
5	11.3	9.0	4.1	1.9	0	0.4	1.0	0.8	2.2
6	17.5	13.9	1.8	1.3	4.3	2.1	0.8	0.8	7.8
7	14.3	9.1	3.1	0.6	2.7	0.5	0.3	0.6	2.9
8	15.9	9.8	2.6	3.0	1.3	1.1	0.8	0.6	3.8
9	14.3	8.9	11.2	0	0	0	2.2	0.6	0.8
10	12.5	7.1	8.9	0	0	0	2.9	0.6	0.8
11	15.8	8.0	2.9	2.7	1.3	1.2	0.8	0.5	2.8

based on powder XRD (Fig. 4). The SEM revealed an interesting distribution of carbonate hydroxylapatite in the plaster surface (Fig. 8). The back-scattered electron image (Fig. 8a) was color-coded for the distribution of three elements: calcium in blue, silicon in red and phosphorus in green (Fig. 8b). Based on this analysis, the surface has a very thin layer of quartz and clays, followed by a 100–150 μm thick layer in which carbonate hydroxylapatite is the main constituent. Below the carbonate hydroxylapatite layer, the major components are the Ca–Si binder with the amorphous silica areas, as described earlier. Samples from upper interfaces of both the upper and lower surfaces were analyzed, and the same carbonated hydroxylapatite distribution was observed.

3.9. Characterization of special features from the shelly layer of the lower surface

The yellow layer, which is part of the 2nd layer of the lower surface (the shelly layer), is silicon-rich and deficient in calcium (Table 1). The yellow color dissolved in HCl. Sulfur was not detected in significant amounts in the yellow samples. In the same layer, but not only in the yellow area, we found several hard, highly porous fragments, around 5 cm in size. Most of these fragments were black, but several were dark green and yellow. Smaller pieces of the same material were present in both layers of the plaster surfaces (for example, features F and I in Fig. 6). Analyses of two of the black fragments are presented in Table 1. The main phase based on infrared analysis, is an amorphous silicate, similar to the spectrum of the plaster itself (Fig. 3). A thin section, observed through polarized light in a petrographic microscope, confirmed that these pieces are not from a volcanic source, and the low iron content implies that they are not by-products of a metal industry.

3.10. Summary

The major phase of the hydraulic plaster is an amorphous silicate which includes hydraulic calcium silicate compounds. The binder is composed of at least 3 different amorphous hydraulic calcium silicate phases, and pyrogenic calcite in a highly disordered state. Additional identified components are quartz grains, geogenic calcite, crushed ceramics, shells (aragonite), carbonate hydroxylapatite, diopside, analcime and pieces of green and dark grey porous glasses containing amorphous silicate and some cristobalite.

4. Discussion

Here we show that these Iron Age plaster surfaces contain a major disordered silicate phase in the binder, in addition to pyrogenic calcite. The presence of this silicate phase proves that this is indeed a hydraulic plaster. In addition, there are larger aggregates composed of a variety of materials. The main question is whether this hydraulic plaster was deliberately prepared based on technical know-how, or it was prepared by chance due to the fortuitous addition of some silicate minerals during the preparation of lime plaster.

We excluded the possibility that the hydraulic plaster was produced by inadvertently heating the local chalky marl, or by the addition of the local clay to calcite. The key to understanding whether the hydraulic plaster was intentionally prepared or not, lies in the additives. The following additives were identified: aragonitic shell fragments, pieces of geologic calcite, quartz, cristobalite, diopside and ceramic sherds. Quartz is a fairly abundant component of the plaster. Significantly, quartz is not abundant in the sediments at the site, and therefore its presence in the plaster implies that it was brought to the site. The coast with its abundant beach sand and shells is just 20 km away. The presence of both quartz sand and marine mollusk shells, suggests that this was one source of additive material.

Cristobalite, a polymorph of quartz, forms at temperatures above 1250 °C. As such high temperatures are not normally achieved during lime plaster production; the cristobalite in the plaster was more likely derived from crushed igneous rock that was added to the plaster before or after calcination. A similar conclusion can be drawn for the diopside, which is a pyroxene mineral also derived from igneous rocks. The closest sources of igneous rocks to the site of Tell es-Safi/Gath are in southern Jordan, the area just north of the Gulf of Aqaba, or the area around Mt. Hermon in the north. These rocks were presumably deliberately brought to the site from these areas, or possibly even from Cyprus or the Aegean.

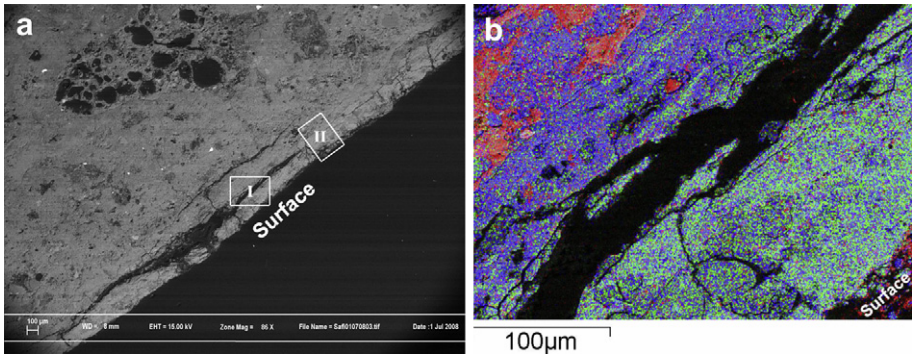

Fig. 8. SEM–EDS analysis of the surface area. (a) A back-scattered electron image of a section of the plaster which includes the surface. Rectangle I is magnified in panel 'b'. Rectangle II was analyzed but not shown here. (b) A magnification of rectangle I in panel 'a'. A color-coded image, using the EDS device. Calcium distribution is in blue, silicon in red, and phosphorus in green. The surface is in the lower right corner.

A second possible silicate source is the hard, porous, black, and green fragments found in and associated with the surfaces, in particular the 2nd layer of the lower surface. Their origin is anthropogenic, probably a waste product of some non-metallurgic industry. An additional source of silicate minerals is the fragments of ceramic sherds (grog). We thus conclude that igneous rock, as well as quartz grains, sherds and shells, were deliberately brought to the site and added to the slaked lime, indicating that the production of this hydraulic plaster was not fortuitous. This conclusion is further supported by the fact that the same plaster was prepared twice at the same location.

A hydraulic plaster is a plaster that can set under water, namely without the uptake of carbon dioxide. There are two different pathways for the formation of hydraulic plasters (Borrelli, 1999; Charola and Henriques, 1999). In the first, designated as 'hydraulic lime' production, calcite (e.g. limestone) and clay are mixed and burned at high temperatures, around 1000–1100 °C. This results in the formation of calcium oxide (quicklime), dicalcium silicate and calcium aluminate. When mixed with water, the products hydrate and set. The minerals formed are calcium silicate hydrates (CSH) and calcium aluminate hydrates (CAH). In the second pathway, designated as 'lime with pozzolanic materials', the calcite is first heated and slaked as in non-hydraulic lime plasters, and then the slaked lime is mixed with pozzolanic additives in the presence of water at ambient temperatures. These include volcanic ash, ground tiles or bricks, pumice, fly ash, opaline materials, certain types of heated clay, etc. The resulting binder compounds are also calcium silicate hydrates (CSH) and calcium aluminate hydrates (CAH), as in the first pathway. In both cases, aluminum can be incorporated in the CSH (Faucon et al., 1999) and the re-formation of calcite from the slaked lime occurs, provided the setting plaster is exposed to air. A characterization of the binder components cannot differentiate unequivocally between these two options. The fact that the shell fragments in the plaster are aragonitic, however, implies that they had to have been added after the calcination process. If the aragonite was heated it would have transformed into calcite. Therefore, this hydraulic plaster was produced using the second pathway.

The authigenic silicate minerals identified in the binder are all consistent with disordered silicate minerals such as those present in powdered igneous rocks and ceramics dissolving and reprecipitating in the high pH environment created by the presence of the slaked lime. Analcime is a zeolitic aluminosilicate mineral with a microporous structure that occurs mainly in volcanic tuffs, but can form naturally when volcanic rocks and ash layers react with alkaline groundwater. Thus the analcime could have been a component of the added igneous rocks, or it could have formed authigenically in the setting plaster. Interestingly, zeolites are high-quality natural pozzolans (Mertens et al., 2009).

These plaster surfaces may have belonged to an installation located in a large courtyard, delimited by the partially excavated buildings (Fig. 2b). Such open courtyards surrounded by buildings are a common phenomenon in the Bronze and Iron Age, and a courtyard with a thick plaster floor was uncovered in the Minoan palace at Petras (Hitchcock, L., pers. observation). Another possibility is that the surfaces belonged to a small, interior room (or installation) that was connected with the processing or collection of liquids in connection with either industrial or hygienic activities (see for example, Mantzourani and Vavouranakis, 2005: 123; Rehak and Younger, 1998: 107; Chapouthier and Charbonneaux, 1928: 36–38; Hitchcock, 2000). The fact that more fragments of these surfaces have not yet been found in the associated fill, may argue for a small room/installation or external space. The sloping surface would have facilitated the drainage or collection of liquids.

The capacity of hydraulic materials to harden under water was widely used for building bridge-footings and harbors (Oleson and Branton, 1992). However, this capacity was probably unnecessary for building household, agricultural or industrial installations, such as the one found in Tell es-Safi/Gath, even if this installation was used for processing liquids. During the Roman period hydraulic plasters were used for various types of structures due to their strength and not only for under water construction (Ward-Perkins, 1981, 97–120). The complex system of preparation layers beneath the plaster surfaces at Tell es-Safi/Gath, was clearly intended to obtain a stable and durable surface.

The archaeological context in which these plaster surfaces were found provides no direct evidence about the activities that took place on them, We did observe that the upper interfaces of the two plaster surfaces have a thin layer of around 150 μm of the phosphate mineral, carbonate hydroxylapatite. We also observed that the distribution of this mineral is related to the distribution of cracks and other internal structures, and that it is also present in the immediate overlying sediments. Thus the phosphate mineral was not added to the plaster as an additional layer, but most probably formed as a result of a reaction between phosphate and the calcite at or just under the upper interface. As the most likely source of phosphate is degrading organic matter, this suggests that organic materials were present on the surfaces. The presence of phosphate minerals in the 10 cm thick layer of sediments above the surface, could imply that these sediments accumulated during or soon after the surfaces were in use.

The documentation of hydraulic plasters from the Iron Age (around 3000 years ago) or from earlier periods is sparse (Chiotis et al., 2001; Dandrau and Dubernet, 2006; Furlan and Bissegger, 1975; Gourdin and Kingery, 1975; Kingery et al., 1988), and there is no clear evidence for a tradition of preparing hydraulic plasters prior to the 5th century BCE. In our opinion this is more likely to reflect the fact that such plasters cannot be identified by visual examination, but require the identification of their mineral components. At Tell es-Safi/Gath, these plasters were identified as part of a survey using FTIR. We note that to date they are the only hydraulic plasters that have been discovered by us at Tell es-Safi/Gath, or at other pre-Roman sites in Israel, where we have carried out similar surveys. Thus, hydraulic plaster production was clearly not common in this region during pre-Roman periods.

A question that arises is the source of the know-how to produce hydraulic plaster at Tell es-Safi/Gath. It can be hypothesized that this know-how was a result of foreign influence. The most likely possible origin of such an influence is the Aegean region, including Crete, which had several natural sources of pozzolanic additives, such as volcanic ash from the island of Thera, although there is no evidence that Santorini earth was used by the Minoans (Shaw, 1971, 210, esp. n. 1). A wide array of plastering technologies serving different purposes (roofing, wall painting, floors, courtyards, cisterns, mortar) was used in the Aegean (Brysbaert, 2008; Dandrau and Dubernet, 2006; Hood and Momigliano, 1994; Shaw, 1971, 207–221, 2006). Chiotis et al. (2001) clearly demonstrate that some of these were hydraulic plasters. Thus the Aegean is a potential source for the transfer of hydraulic plaster technology to the southern Levant.

5. Conclusions

Hydraulic plaster, approximately 3000 years old was deliberately made by the addition of crushed ceramics, powdered igneous rocks and possibly silicate industrial waste, serving as pozzolanic materials. The use of these hydraulic plaster surfaces is not clear, although the presence of carbonate hydroxylapatite on the surfaces and the immediate area indirectly implies the involvement of

organic materials. These are the only samples of Philistine hydraulic plasters analysed to date, and are one of the earliest, if not the earliest, definitively characterized hydraulic plasters known. These plasters demonstrate the high degree of sophistication of the Iron Age Philistine culture.

Acknowledgements

Special thanks are due to Ruth Shahack-Gross and Panagiotis Karkanas for useful discussions of the data, to Adi Eliyahu-Behar and Ellen Pechtel for their assistance with the XRF and pXRD devices respectively, to P. Tiano for the pozzolana and cement samples, and to Leon Cherniaev, Yotam Asscher, Jeffrey Dobereiner, Brent Davis, Sam Crooks, and Sarah Klavins for assistance in the field. The research leading to these results has received funding from the European Research Council under the European Community's Seventh Framework Programme (FP7/2007-2013)/ERC grant agreement no 229418.

References

Berna, F., Behar, A., Shahack-Gross, R., Berg, J., Boaretto, E., Gilboa, A., Sharon, I., Shalev, S., Shilshtein, S., Yahalom-Mack, N., Zorn, J.R., Weiner, S., 2007. Sediments exposed to high temperatures: reconstructing pyrotechnological processes in Late Bronze and Iron Age Strata at Tel Dor (Israel). Journal of Archaeological Science 34, 358–373.

Borrelli, E., 1999. Binders-ARC Laboratory Handbook, ICCROM ARC Laboratory Handbook. ICCROM, Rome.

Boynton, R.S., 1980. Chemistry and Technology of Lime and Limestone. John Wiley & Sons, New York.

Brysbaert, A., 2008. The Power of Technology in the Bronze Age Eastern Mediterranean. The Case of Painted Plaster. In: Monographs in Mediterranean Archaeology, vol. 12 London and Oakville.

Chapouthier, F., Charbonneaux, J., 1928. Fouilles exécutées à Mallia I. Études Crétoises 1 Paris.

Charola, A.E., Henriques, F.M.A., 1999. Hydraulicity in Lime Mortars Revisited. In: Bartos, P.J.M., Groot, C.J.W., Hughes, J.J. (Eds.), Proceedings of RILEM International Workshop Historic Mortars: Characteristics and Tests, Paisley, pp. 97–106.

Chiotis, E., Dimou, E., Papadimitriou, G.D., Tzoutzopoulos, S., 2001. The Study of Some Ancient and Prehistoric Plasters and Watertight Coatings from Greece. In: Aloupi, E., Bassiakos, Y., Facorellis, Y. (Eds.), Archaeometry Issues in Greek Prehistory and Antiquity. Hellenic Society for Archaeometry and the Society of Messenean Archaeological Studies, Athens, pp. 327–342.

Chu, V., Regev, L., Weiner, S., Boaretto, E., 2008. Differentiating between anthropogenic calcite in plaster, ash and natural calcite using infrared spectroscopy: implications in archaeology. Journal of Archaeological Science 35, 905–911.

Dandrau, A., Dubernet, S., 2006. Plasters from Kommos: A Scientific Analysis of Fabrics and Pigments. In: Shaw, J. (Ed.), Kommos 5: The Monumental Minoan Buildings at Kommos. Princeton University Press, Princeton, pp. 236–241.

Faucon, P., Delagrave, A., Petit, J.C., Richet, C., Marchand, J.M., Zanni, H., 1999. Aluminum incorporation in calcium silicate hydrates (C-S-H) depending on their Ca/Si ratio. Journal of Physical Chemistry B 103 (37), 7796–7802.

Fiandra, E., 1961–1962. I Periodi struttivi del Primo Palazzo di Festòs. Kritika Chronika 15–16 (A), 112–126.

Furlan, V., Bissegger, P., 1975. Les mortiers anciens. Histoire et essais d'analyse scientifique. Revue suisse d'Art et d"Archéologie 32, 166–178.

Gourdin, W., Kingery, W., 1975. The beginnings of pyrotechnology: Neolithic and Egyptian lime plaster. Journal of Field Archaeology 2 (1/2), 133–150.

Gueta, R., Natan, A., Addadi, L., Weiner, S., Refson, K., Kronik, L., 2007. Local atomic order and infrared spectra of biogenic calcite. Angewandte Chemie International Edition 46, 291–294.

Hancock, R.G.V., 2003. Elemental Analysis of Local Limestone and Prepared Plaster Samples. In: Daviau, P.M.M. (Ed.), The Iron Age Town. Excavations at Tall Jawa, Jordan, vol. I, Leiden, pp. 457–463.

Hitchcock, L.A., 2000. Of Bar Stools and Beehives: An Interpretive Dialog About a Minoan Store Room. In: Proceedings of the Eighth International Congress of Cretan Studies A.1. Heraklion, 593-606, 9–14 September 1996.

Hood, S., Momigliano, N., 1994. Excavations of 1987 on the south front of the palace at Knossos. Annual of the British School at Athens 89, 103–150.

Karkanas, P., Rigaud, J.P., Simek, J.F., Albert, R.M., Weiner, S., 2002. Ash, bones and guano: a study of the minerals and phytoliths in the sediments of Grotte XVI, Dordogne, France. Journal of Archaeological Science 29, 721–732.

Kingery, W., Vandiver, P., Prickett, M., 1988. The beginnings of pyrotechnology, part II: production and use of lime and gypsum plaster in the pre-pottery Neolithic near east. Journal of Field Archaeology 15 (2), 219–244.

Levi, D., 1964. The Recent Excavations at Phaistos. In: Studies in Mediterranean Archaeology 11 Lund.

Maeir, A.M., 2008. Zafit, Tel. In: Stern, E. (Ed.), The New Encyclopedia of Archaeological Excavations in the Holy Land, vol. 5: Supplementary Volume, Jerusalem, pp. 2079–2081.

Maeir, A.M., Wimmer, S.J., Zukerman, A., Demsky, A., 2008. A Late Iron Age I/Early Iron Age II Old Canaanite inscription from Tell esi-Sâfī/Gath, Israel: palaeography, dating, and historical-cultural significance. Bulletin of the American Schools of Oriental Research 351, 39–71.

Mantzourani, E., Vavouranakis, G., 2005. Achladia and Epano Zakros: a re-examination of the architecture and topography in two possible Minoan villas in east crete. Opuscula Atheniensia 30, 99–125.

Mertens, G., Snellings, R., Van Balen, K., Bicer-Simsir, B., Verlooy, P., Elsen, J., 2009. Pozzolanic reactions of common natural zeolites with lime and parameters affecting their reactivity. Cement and Concrete Research 39 (3), 233–240.

Oleson, J.P., Branton, G., 1992. The Technology of King Herod's Harbor. In: Vann, R.L. (Ed.), Caesarea Papers: Straton's Tower, Herod's Harbour, and Roman and Byzantine Caesarea, Ann Arbor, pp. 56–65.

Rehak, P., Younger, J., 1998. Review of Aegean prehistory VII: Neopalatial, final palatial, and postpalatial crete. American Journal of Archaeology 102, 91–173.

Shaw, J.W., 1971. Minoan architecture: materials and techniques. Annuario 49 Rome.

Shaw, M.C., 2006. Plasters from the Monumental Minoan Buildings: Evidence for Painted Decoration, Architectural Appearance, and Archaeological Event. In: Shaw, J.W., Shaw, M.C. (Eds.), Kommos 5. The Monumental Minoan Buildings at Kommos, Princeton, pp. 117–229.

Valla, F.R., Khalaily, H., Valladas, H., Kaltnecker, E., Bocquentin, F., Cabellos, T., Bar-Yosef Mayer, D.E., Le Dosseur, G., Regev, L., Chu, V., Weiner, S., Boaretto, E., Samuelian, N., Valentin, B., Delerue, S., Poupeau, G., Bridault, A., Rabinovich, R., Simmons, T., Zohar, I., Ashkenazi, S., Delgado Huertas, A., Spiro, B., Mienis, H.K., Rosen, A.M., Porat, N., Belfer-Cohen, A., 2007. Les Fouilles de Ain Mallaha (Eynan) de 2003 à 2005: Quatrième Rapport Préliminaire. Mitekufat Haeven-Journal of the Israel Prehistoric Society 37, 135–383.

Walberg, G., 2001. The role and Individuality of kamares ware. Aegean Archaeology 5, 9–18.

Ward-Perkins, J.B., 1981. Roman Imperial Architecture, second ed. Harmondsworth.

Wright, J.C., 1978. Mycenaean Masonry Practices and Elements of Construction. Unpublished Ph.D. Dissertation, Bryn Mawr College, USA.

Wright, G.R.H., 2000. Ancient Building Technology, vol. 1 Historical Background, Leiden.

Wright, G.R.H., 2005. Ancient Building Technology, vol. 2 Materials, Part 1: Text, Leiden.

Zukerman, A., Maeir, A.M. The Stratigraphy and Architecture of Area A. Excavations at Tell es-Safi/Gath, Volume 1. Maeir, A.M. (Ed.). AAT 69. Wiesbaden, in press.